

Machine learning for interpreting coherent X-ray speckle patterns

Mingren Shen¹, Dina Sheyfer², Troy David Loeffler³, Subramanian K.R.S. Sankaranarayanan^{3,5}, G. Brian Stephenson⁴, Maria K. Y. Chan³, Dane Morgan¹

¹ Department of Materials Science and Engineering, University of Wisconsin-Madison, Madison, Wisconsin, 53706, USA

² X-ray Science Division, Argonne National Laboratory, Lemont, IL 60439, USA

³ Center for Nanoscale Materials, Argonne National Laboratory, Lemont, Illinois 60439, USA

⁴ Materials Science Division, Argonne National Laboratory, Lemont, IL 60439, USA

⁵ Department of Mechanical and Industrial Engineering, University of Illinois, Chicago IL – 60607, USA

Abstract

Speckle patterns produced by coherent X-ray have a close relationship with the internal structure of materials but quantitative inversion of the relationship to determine structure from images is challenging. Here, we investigate the link between coherent X-ray speckle patterns and sample structures using a model 2D disk system and explore the ability of machine learning to learn aspects of the relationship. Specifically, we train a deep neural network to classify the coherent X-ray speckle pattern images according to the disk number density in the corresponding structure. It is demonstrated that the classification system is accurate for both non-disperse and disperse size distributions.

1. Introduction

Current and developing X-ray sources such as the advanced synchrotron sources, X-ray free electron lasers, and high harmonic generation sources^{1,2} enable utilization of coherent x-ray light to investigate behavior in the time domain and structure at interatomic length scales. For example, X-ray photon correlation spectroscopy has been used by many researchers in materials science, including investigations of micro, nano, and atomic scale structures^{3,4} and mechanisms⁵, studying dynamics and correlation behaviors^{6–8}, revealing rich phenomena in complex material systems, e.g. multicomponent fluids⁹ and metallic glasses¹⁰, and in other areas. Coherent X-ray imaging methods have been used in many materials applications to visualize the chemical composition at nanoscale resolution^{11,12} and to study 3D lattice dynamics in nanocrystals¹³, and in biology to image the 3D mass density distribution of a whole cell¹⁴, and to reconstruct the 3D structure of the giant mimivirus particle¹⁵.

Coherent X-rays incident on a disordered sample generate X-ray speckle patterns, which are often difficult to interpret, especially to reconstruct molecular structure from the image. Such reconstructions to date have often relied on complex, subjective algorithms or required multiple experiments, e.g., using phase retrieval algorithms to iterate between real and reciprocal space^{16,17} or alternating projections¹⁸, angles or sample positions¹⁹. The reconstruction problem occurs because only amplitude information is recorded in the detector and additional computation is required to recover phase information. Deep learning, if used properly, has been shown to be able to learn complex mapping between input space and output space automatically from data²⁰ and has been widely used for physics^{21–24}, chemistry²⁵, materials science^{26–29}, health industry,^{30–32} etc. It is therefore of interest to explore whether recent developments in image analysis using machine learning might aid in the extraction of structural information from X-ray speckle patterns.

Machine learning or deep learning methods can help X-ray speckle pattern problems in three aspects, namely data collection, data transformation, and data analysis. For data collection, the main goal is to acquire high resolution and lower noise images. Konstantinova et al. use a convolutional neural-networks-based encode-decoder framework to reduce noises in X-ray images³³ and Cherukara et al. use neural networks to boost low resolution scanning coherent diffraction images to high fidelity ones³⁴. Other

ideas like developing a novel machine-learning-based data acquisition process to interpret common nanoscale lattice structural distortions³⁵ and using deep reinforcement learning to help lower dose used for ptychography experiments³⁶ also show great promise. For data transformation, the aim is preprocessing raw data to get prepared data for analysis. For example, neural-network-based data augmentation methods are used to increase data volume,^{37,38} and physics information such as geometry³⁹ and spherical harmonics for representing crystals⁴⁰ are incorporated into machine learning methods to get better performance. A machine-learning-based automatic X-ray scattering image annotation system has also been developed by Guan et al. to help increase the speed of data ingestion⁴¹. For data analysis, more powerful machine learning models⁴²⁻⁴⁴, better features⁴⁵, and new templates⁴⁶ have all been attempted for various tasks showing promising advantages compared to traditional methods^{34,35,37,39,42}.

For this study, the major challenge impeding the application of supervised machine learning or deep learning methods for X-ray speckle pattern problems⁴⁷ is a lack of labeled data for training, since we generally have little or no knowledge of ground truth values for the real physical systems being characterized. Two general approaches to overcoming this challenge are (i) to use synthetic data, e.g., generated by forward simulation of relevant molecular structures, and (ii) to make extremely efficient use of data that is available through approaches like transfer learning, few shot learning, physics guided models, and data augmentation. The two approaches can certainly be used together. We take approach (i) in the present work, demonstrating that we can effectively use machine learning to extract structural information from simulated speckle patterns derived from simplified forward simulation on a very idealized model system. However, this is a very preliminary step, and a combination of more physically realistic synthetic data, experimental data, and highly data efficient machine learning approaches will likely be needed to realize practical models. To better focus on examining machine learning model's ability to interpret speckle patterns, we use a simple 2D disks system to generate speckle patterns, however, more realistic synthetic data of speckle patterns could be obtained from better materials simulation methods such as Molecular Dynamics (MD) or Kinetic Monte Carlo (KMC)⁴⁸⁻⁵⁰.

In this study, we explore the ability of machine learning to learn aspects of the relationship between coherent X-ray speckle patterns and sample structures using a model 2D disk system. Specifically, we train a deep neural network to classify the coherent X-ray speckle patterns according to the disk number density in the corresponding structure. Disk number density is one of the simplest and most direct properties to determine and is analogous to number densities often of interest in colloidal systems. We therefore consider it a good property for an initial exploration of the capabilities of deep learning for this problem. We focus on a representative 2D system to allow a more rapid study at this initial stage, although extension to 3D systems is straightforward and clearly a valuable focus for future work. The classifier was trained on simulated coherent X-ray speckle patterns without any assumptions or simplifications and the results suggest that it is possible to use machine learning tools to correlate coherent X-ray speckle patterns to structural or particle distribution information with machine learning. The method directly builds a mapping between the k -space coherent X-ray speckle patterns and real-space sample information, e.g., disk number density. The present model is trained on synthetic data for an idealized system and therefore not directly applicable to speckle patterns from physical samples. However, its success suggests that, if accurate training data can be obtained, a deep learning algorithm could be developed to aid in structural analysis from speckle patterns in real systems. In the discussion, we compare the results to a conventional x-ray scattering analysis.

2. Material and methods

Overview

We used forward-simulation methods to generate coherent X-ray speckle pattern images of a model 2D disk system and then trained a Convolutional Neural Network (CNN) model called Resnet-50 to classify the X-ray speckle patterns into different categories corresponding to their disk numbers. The workflow pipeline of this approach is shown in Figure 1. The generated speckle pattern images were used as input images and the disk number density as the target class. These were then used to train the Resnet-50 network to classify a speckle pattern by its number density.

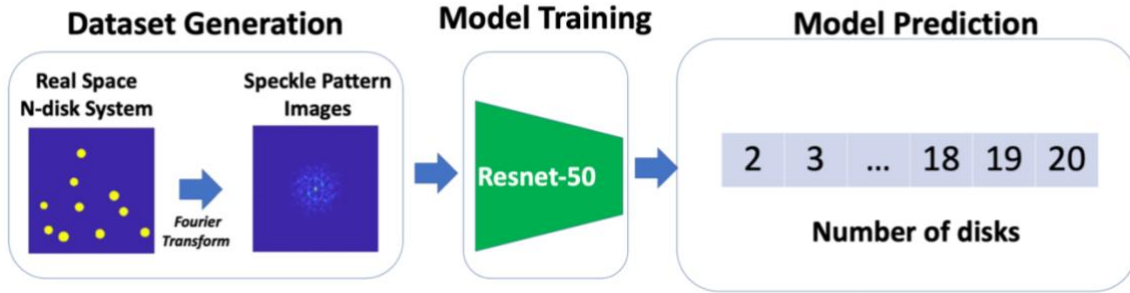


Figure 1. Flow chart of machine learning system which includes dataset generation, model training and model prediction and interpretation.

Model system generation

The 2D system used in our study was 2000 x 2000 units in real space and the total area of disks is kept at a constant (equal to $2 \times \pi \times 90 \times 90 = 16200\pi$ where 90 is the radius of the two-disk system). For an n -disk system, the radius of each disk was set to preserve the total area of disks, which requires $r = \sqrt{\frac{16200}{n}}$. Then the n disks were randomly placed into the 2D box without overlap of disks. For a select set of studies focused on polydispersity, the single radius system of n disks was modified by sampling the radii from a Gaussian distribution of a given mean and standard deviation with the constraint that the total area of disks is kept the same as the original single radius n -disk system (16200π). The standard deviation was chosen to be 1/3 of the mean to represent a significant but not overwhelming spread in particle sizes compared to the mean, as might be seen in a real nanocluster system.

Speckle pattern dataset generation

To generate X-ray speckle pattern data, we use a Fourier Transform to convert the 2D n -disk system of real space to the reciprocal (k) space images. The width of each side of a pixel in k space is $w = \pi/L$ where L is the size of the real space image. Each pixel in the X-ray speckle patterns is centered around the k -space coordinate used to calculate the Fourier transform for that pixel. The k -space coordinates are of the form $(n_x \times w, n_y \times w)$, where n_x and n_y are integers ranging from 0 to n_{max} , and n_{max} can be 256 or

512, yielding images of size 257×257 and 513×513 , respectively. The k-space images range along each axis is from 0 to k_{max} , where $k_{max} = \frac{n_{max} \times \pi}{L}$. In *Figure 2* we show real space and corresponding k space images for select n-disk systems ($n = 2, 3, 6, 10, 15, 20$). For clarity, all k space images arbitrarily scaled to highlight the speckle patterns. In total we consider 19 cases given by $n = 2-20$.

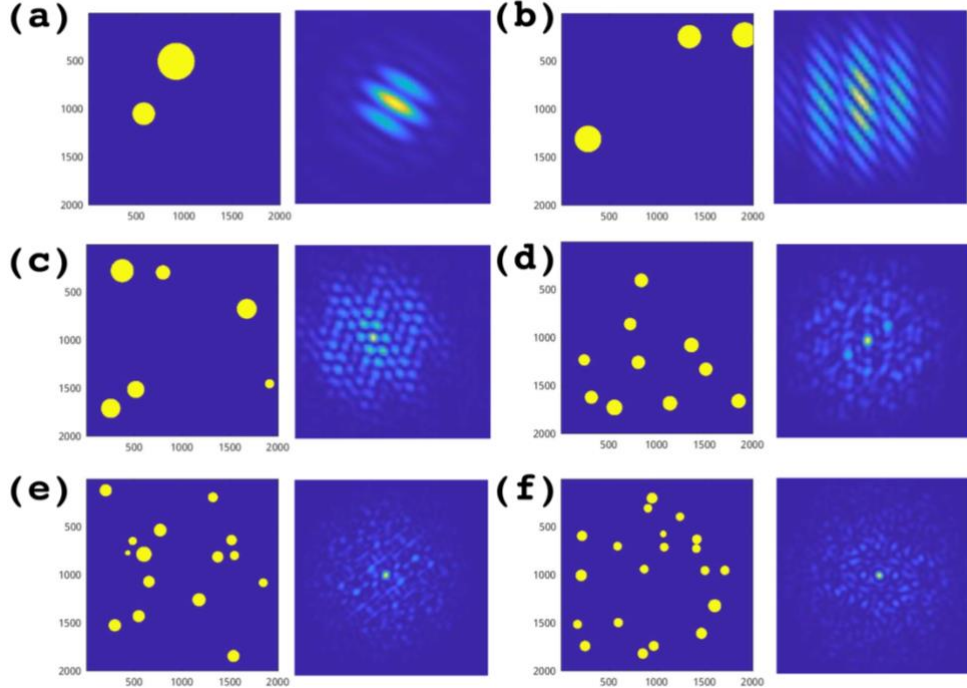


Figure 2. Real space images and corresponding X-ray speckle patterns, arbitrarily scaled to highlight the speckle patterns for six typical 2D disk system with (a) 2-disks, (b) 3-disks, (c) 6-disks, (d) 10-disks, (e) 15-disks, and (f) 20-disks.

Data processing

After obtaining the X-ray speckle patterns, some preprocessing was performed. The 11 pixels x 11 pixels center region of the X-ray speckle patterns was blocked to mimic what is commonly done in experiments to avoid the excessive brightness of the center pixels¹⁹. Standardization was applied to each image to make sure the pixel intensity of all speckle pattern images has the zero mean and unit variance. This is an important step to remove any correlation between the overall intensity and the number density

of disks to ensure the machine learning system is forced to focus on the structure of X-ray patterns rather than the intensity distribution. This standardization mimics what would be needed in real data where the contrast of the objects is typically unknown.

Machine learning model and data: properties, fitting, and analysis

We applied the widely used CNN model called ResNet-50 to classify the speckle pattern images based on the number of disks. ResNet^{51,52} is a family of deep learning models that use identity mappings to overcome the performance degradation problem of stacking more layers⁵³. It is the first deep learning model that achieved lower than human level error rate in the ImageNet Large Scale Visual Recognition Challenge (ILSVRC) 2015 competition⁵⁴. For this work, we created 1000 different random configurations of disk position each for 19 different disk numbers. In total, we have 19000 X-ray speckle pattern images and among them, 15200 images were used for training, 1900 images were used for validation, and the remaining 1900 images were used for testing. The 1900 image test set contain exactly 100 images for each disk number 2-20 to keep testing unbiased. This condition was enforced by randomly selecting 100 images from the 1000 total images of each disk number to build the test set. The training and validation set were randomly split from the remaining 17100 images after the test set was extracted. ResNet-50 model was written in Keras⁵⁵ with TensorFlow⁵⁶ as the backend engine and the training used the Adam optimizer and categorical cross entropy loss with default setting of Keras. A typical training used 200 epochs with batch size of 40.

To estimate the performance of our models, we will use precision, recall, and F1 scores. Here precision means the ratio between correct classified speckle patterns over all predicted speckle patterns, recall means the ratio between correct classified speckle patterns over all testing speckle patterns, and F1 scores is the harmonic mean of precision and recall.

3. Results

We first present the non-polydisperse system results where all disks were the same size in each image and then we show the polydisperse system results where disk sizes in an image follow a Gaussian distribution (the construction of the polydisperse system was discussed in Section 2).

3.1 Non-Polydisperse System Results

The non-polydisperse classification results on test data for 19 different disk numbers are shown in Figure 3. Figure 3 demonstrates that the classification algorithm works extremely well. Misclassification only happens once, in the case of 19 disks, which only shows a small error by misclassifying 19 as 18. This one error is the only misclassification in all 1900 test cases. The cross-class accuracy is nearly 99.9% which demonstrates the capacity of the present Resnet-50 based deep learning classification system to extract structural information from X-ray speckle patterns, at least when sufficient training data is available.

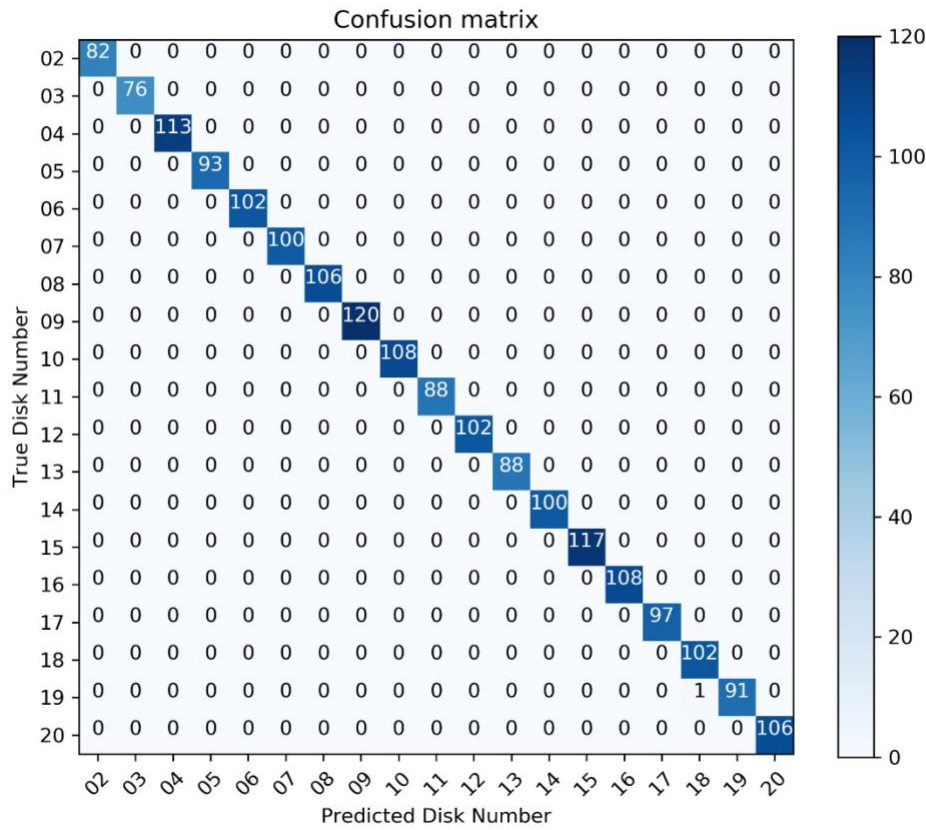


Figure 3. Confusion Matrix of non-polydispersity system classification results using 257×257 as input coherent X-ray speckle pattern image size.

In examples above, we focused on 257×257 pixel size as the coherent X-ray inputs, and it is important to know that whether different size of inputs will change the classification results. We increased the number of pixels from 257×257 to 513×513 , which, following the k-space scheme described in the Methods section, effectively doubled the range of k values sampled but kept the sampling density the same. This change added many higher k values, or equivalently, extended the sampling to smaller distances in real space (specifically, exploring the additional real space ranges of $2L/256$ down to $2L/512$). We applied the exact same neural network that was obtained from training on the 257×257 images to classify the 513×513 images. We show the confusion matrix of 513×513 pixel size inputs in Figure 4,

which shows few changes compared to Figure 3. The drop of performance corresponds to three misclassifications compared to just one from the smaller images used previously, which is a very modest increase in error. This result indicates that the 257×257 pixel image reaches high enough k values for our classification problem, even though the larger size inputs have more information.

In summary, the deep learning classifier works very well for identifying the number of disks from coherent X-ray speckle patterns in our model non-polydisperse systems.

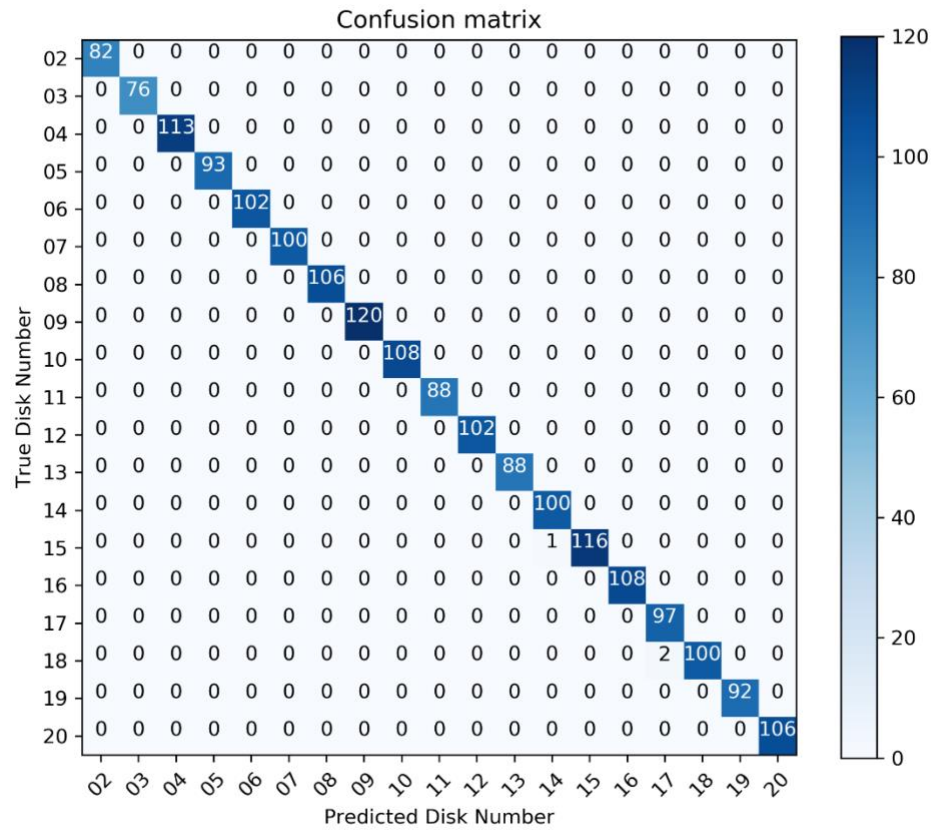


Figure 4. Confusion Matrix of non-polydispersity system classification results using 513×513 as input coherent X-ray speckle pattern image size.

3.2 Polydisperse System Results

In Section 3.1, we presented results of the deep learning classifier for coherent X-ray speckle patterns in non-polydisperse systems. However, real systems will always have some dispersion, so to further test the capacity of the classifier, we retrained the model and tested it on a polydisperse dataset (see Methods for how the polydisperse dataset was constructed). Figure 5 shows the confusion matrix of the polydisperse classifier. There is a significant performance drop compared to non-polydisperse results. Table 1 shows class specific precision, recall, F1 scores. The cross-class precision, recall and F1-score are all 0.89, lower than the non-polydisperse system due to the drop of performance in larger disk number systems from 14 to 20. The performance is still generally quite good, with only 18 cases out of 1900 showing errors more than one disk, and only one case of 1900 showing errors more than 2 disks.

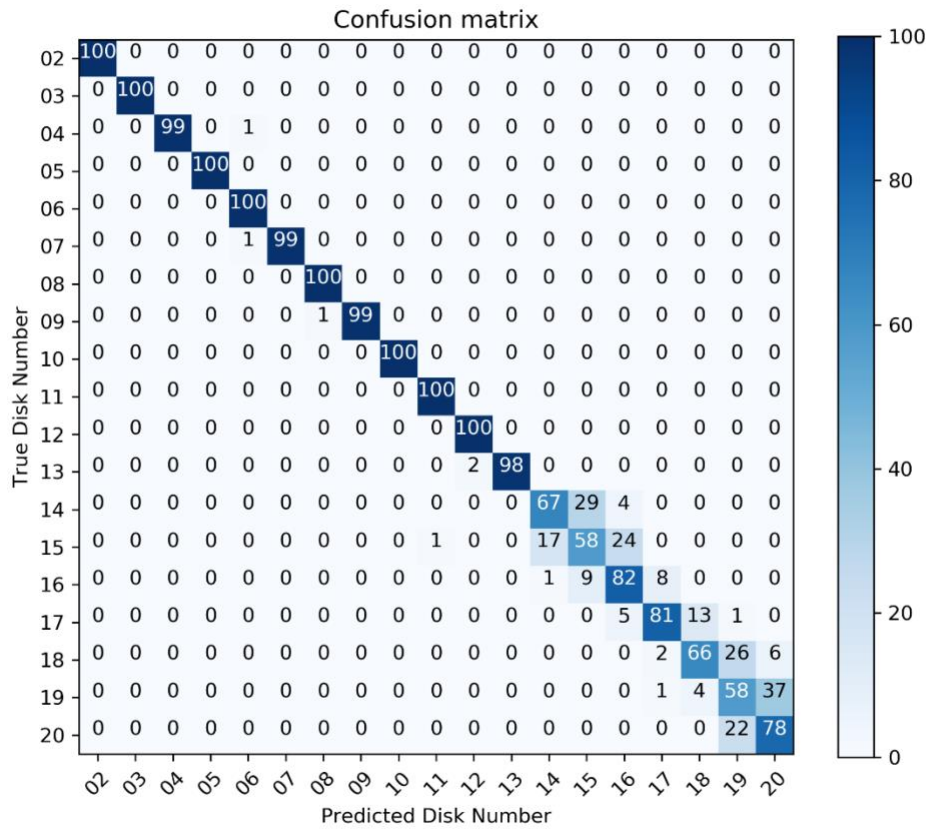


Figure 5. Confusion Matrix of polydispersity system classification results using 257×257 as input coherent X-ray speckle pattern image size.

Table 1. Classification performance for different polydispersity disk numbers.

Disk Numbers	precision	recall	F1-score
Disks_02	1	1	1
Disks_03	1	1	1
Disks_04	1	0.99	0.99
Disks_05	1	1	1

Disks_06	0.98	1	0.99
Disks_07	1	0.99	0.99
Disks_08	0.99	1	1
Disks_09	1	0.99	0.99
Disks_10	1	1	1
Disks_11	0.99	1	1
Disks_12	0.98	1	0.99
Disks_13	1	0.98	0.99
Disks_14	0.79	0.67	0.72
Disks_15	0.6	0.58	0.59
Disks_16	0.71	0.82	0.76
Disks_17	0.88	0.81	0.84
Disks_18	0.8	0.66	0.72
Disks_19	0.54	0.58	0.56
Disks_20	0.64	0.78	0.71

4. Discussion and Summary

We developed a deep learning based model to identify disk number by classification from coherent X-ray speckle patterns of a two dimensional disk model system. The classifier was tested with and without dispersity and shown to be effective in both cases, although systems with polydispersity show significant errors depending on the scale of the dispersity. Overall, our results demonstrate that without using complex experimental procedures e.g., taking multiple images in different angles or positions for phase retrieval, or pre-defined assumptions about samples, we could directly extract real space sample information such as number density from k-space X-ray speckle patterns.

The way we generated the disk systems produced a direct correlation between the average disk size and the average disk number density. Since the average disk size can be estimated from conventional X-ray scattering analysis, we also conducted a comparison of our ML-based analysis with conventional analysis. Conventional X-ray scattering analysis would determine the average disk number density by looking at the overall width of the scattering; smaller disks would give a broader width. We quantify the overall width of the scattering by its first moment, i.e., the average of the product of the pixel intensity and its distance from $q = 0$, typically divided by the average intensity. We determine the first moment on the same images used for the ML (specifically, the images had central regions removed and intensities standardized, as discussed in Sec. 2) as well as ones without standardization. Below we will use 513 \times 513 Non-Polydisperse System, since it shows good performance, to show the relationship between mean first moment and disk number in raw speckle intensity and standardized speckle intensity. Our ML system uses standardization as preprocessing for images which makes some intensities zero and some negative and thus creates some uncertainty in how to analyze the first moment of the standardized images. Therefore, we will show two different definitions of approximated first moment for standardized speckle images. The first definition, which we refer to as using “shifted standardized” data, is just the average of the product of the pixel intensity and its distance from $q = 0$ divided by the average intensity plus one to avoid dividing by zero. The second definition, which we refer to as using “absolute standardized” data, is the average of the product of the absolute value of pixel intensity and its distance from $q = 0$ to make sure negative pixel intensity does not cancel positive intensity. Since in X-ray width analysis, normalized raw intensity to 0~1 range is often used, we also present normalized intensity results of using Min-Max Scaler, $(I - I_{min})/(I_{max} - I_{min})$, which is referred as “normalized standardized” data. We select 10 speckle pattern images for each disk number and show both the raw scatter point plot and the aggregated plot of the mean of those 10 images in Figure 6.

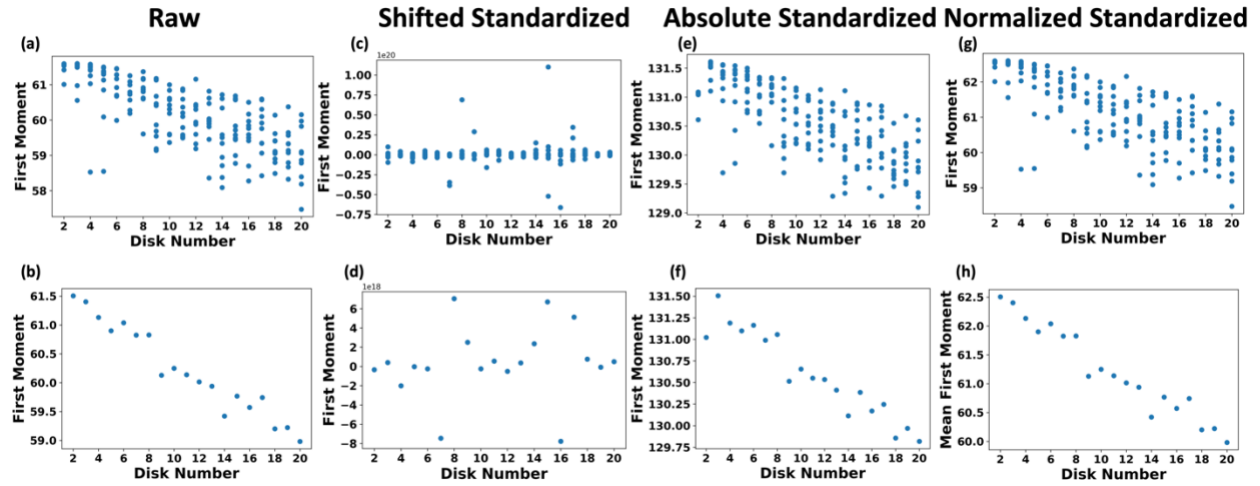


Figure 6. Relationship between first moment and disk number in raw intensity, shifted standardized, absolute standardized and normalized standardized ML data. (a), (c), (e), (g) show the 10 sampled speckle images, and (b), (d), (f), (h) show the mean value of those 10 samples.

Figure 6(a) shows a clear relationship between mean first moment and disk number. This relationship is largely lost for the shift standardized data (Figure 6(c)) but still quite strong in the absolute standardized data (Figure 6(e)) and normalized standardized data (Figure 6(g)). This result provides evidence that there is indeed relationship between disk number and intensity in the data which the ML can learn. While this analysis shows that first moment and disk number are related, the large scatter in all the cases Figure 6(a,c,e,g), and particularly for shifted standardized data, means that many samples must be taken for a given disk count to robustly estimate the disk count value. However, our ML model can do this with just one image, demonstrating it is much more powerful than just the first moment.

It is also of interest to explore those aspects of the speckle pattern are being used by the ML model in determining disk count. To explore this question, we applied Saliency Maps⁵⁷ and Gradient-weighted Class Activation Mapping (Grad-CAM)⁵⁸, two widely used techniques to analyze CNN based image classification system, which can give insight into the pixel regions that are important for final

classifications. Although Grad-CAM and Saliency Map have been used for interpretations of natural images^{59,60}, photovoltaics⁶¹, small angle X-ray diffraction data³⁷ and galaxy evolution⁶², the results from coherent X-ray speckle images did not point us to any clear interpretations of what pixels were being used to identify which categories. We attach results of Saliency Map and Grad-CAM results in SI for further references.

Although the present results are encouraging, significantly more work is needed to assure that machine learning models can be used to aid in interpretation of spectral patterns. First, real coherent X-ray images have noise due to environments, devices, detectors etc. The impacts of noise on the classification need to be assessed, although it is likely that this does not represent a fundamental challenge. We expect that enough data with well-enough controlled noise will yield robust models, as found for most of the data here. Second, our model loses accuracy in larger and polydisperse systems, which is likely due at least in part to having many disks with different sizes that blur peaks and thus make it hard to discover patterns. This problem could potentially be reduced by adding more training images for larger disk numbers. A closely related third limitation is that it is still unclear what kinds of training are needed to enable extraction of useful data e.g., how many training images are needed to train a successful speckle pattern extraction model. Perhaps most importantly, it is not clear how such training data can be practically obtained. The data would likely have to be obtained using systems with ground-truth properties accessible by some other method, perhaps aided by other experiments to find those properties, or simulations where all the properties are readily available. One might consider using data from colloidal systems, which are relatively easy to investigate⁶³. Finally, we note a fourth limitation which is that our system is a model 2D system. Machine learning approaches should be tested on data of 3D systems and if possible, tested with relevant experimental data. Despite these many limitations, the success of these initial results suggests that further related studies may be fruitful.

Data And Code Availability

The data described in the Supporting Information and the data used in plotting all figures in manuscript are available at Figshare (<https://doi.org/10.6084/m9.figshare.16850398.v3>). The Supporting Information data includes Saliency Map Images and Class Activation Map (CAM) Images for both non-polydisperse systems of size 257×257 and 513×513 , and a polydisperse system with size 257×257 .

The source code for generating the X-ray speckle pattern images, training Resnet based classification, and analyzing classification results are available on GitHub (<https://github.com/uw-cmg/ML4XraySpecklePattern>).

Competing Interests

There are no competing interests in relation to the work described.

Acknowledgments

This material is based upon work supported by Laboratory Directed Research and Development (LDRD) funding from Argonne National Laboratory, provided by the Director, Office of Science, of the U.S. Department of Energy (DOE) under Contract No. DE-AC02-06CH11357. Use of the Center for Nanoscale Materials, an Office of Science user facility, was supported by the DOE, Office of Science, Office of Basic Energy Sciences (BES), under Contract No. DE-AC02-06CH11357. X-ray analysis was supported by DOE BES Materials Sciences and Engineering. We would like to thank the Wisconsin Applied Computing Center (WACC) for providing access to the CPU/GPU cluster, Euler. Special thanks to Colin Vanden Heuvel for helping us use GPUs and install the required software.

Reference

1. Miao, J., Ishikawa, T., Robinson, I. K. & Murnane, M. M. Beyond crystallography: Diffractive imaging using coherent X-ray light sources. *Science* (1979) **348**, 530–535 (2015).
2. Chapman, H. N. X-ray imaging beyond the limits. *Nature Materials* 2009 **8**:4 **8**, 299–301 (2009).
3. Brisard, S., Serdar, M. & Monteiro, P. J. M. Multiscale X-ray tomography of cementitious materials: A review. *Cem Concr Res* **128**, 105824 (2020).
4. Vicente, R. A., Neckel, I. T., Sankaranarayanan, S. K. R. S., Solla-Gullon, J. & Fernández, P. S. Bragg Coherent Diffraction Imaging for in Situ Studies in Electrocatalysis. *ACS Nano* vol. 15 6129–6146 Preprint at <https://doi.org/10.1021/acsnano.1c01080> (2021).
5. Leitner, M., Sepiol, B., Stadler, L.-M., Pfau, B. & Vogl, G. Atomic diffusion studied with coherent X-rays. *Nature Materials* 2009 **8**:9 **8**, 717–720 (2009).
6. Madsen, A., Fluerasu, A. & Ruta, B. Structural Dynamics of Materials Probed by X-Ray Photon Correlation Spectroscopy. *Synchrotron Light Sources and Free-Electron Lasers: Accelerator Physics, Instrumentation and Science Applications* 1617–1641 (2016) doi:10.1007/978-3-319-14394-1_29.
7. Boldon, L., Laliberte, F. & Liu, L. Review of the fundamental theories behind small angle X-ray scattering, molecular dynamics simulations, and relevant integrated application. <http://dx.doi.org/10.3402/nano.v6.25661> **6**, 25661 (2015).
8. Sandy, A. R., Zhang, Q. & Lurio, L. B. Hard X-Ray Photon Correlation Spectroscopy Methods for Materials Studies. <https://doi.org/10.1146/annurev-matsci-070317-124334> **48**, 167–190 (2018).
9. Sheyfer, D. *et al.* Nanoscale Critical Phenomena in a Complex Fluid Studied by X-Ray Photon Correlation Spectroscopy. *Phys Rev Lett* **125**, 125504 (2020).
10. Evenson, Z. *et al.* X-Ray Photon Correlation Spectroscopy Reveals Intermittent Aging Dynamics in a Metallic Glass. *Phys Rev Lett* **115**, 175701 (2015).
11. Jiang, H. *et al.* Three-Dimensional Coherent X-Ray Diffraction Imaging of Molten Iron in Mantle Olivine at Nanoscale Resolution. *Phys Rev Lett* **110**, 205501 (2013).
12. Zhao, Y. *et al.* A Polymerization-Assisted Grain Growth Strategy for Efficient and Stable Perovskite Solar Cells. *Advanced Materials* **32**, 1907769 (2020).
13. Clark, J. N. *et al.* Ultrafast Three-Dimensional Imaging of Lattice Dynamics in Individual Gold Nanocrystals. *Science* (1979) **341**, 56–59 (2013).
14. Jiang, H. *et al.* Quantitative 3D imaging of whole, unstained cells by using X-ray diffraction microscopy. *Proceedings of the National Academy of Sciences* **107**, 11234–11239 (2010).
15. Ekeberg, T. *et al.* Three-Dimensional Reconstruction of the Giant Mimivirus Particle with an X-Ray Free-Electron Laser. *Phys Rev Lett* **114**, 098102 (2015).
16. Lohse, L. M. *et al.* A phase-retrieval toolbox for X-ray holography and tomography. <urn:issn:1600-5775> **27**, 852–859 (2020).
17. Maddali, S. *et al.* Phase retrieval for Bragg coherent diffraction imaging at high x-ray energies. *Phys Rev A (Coll Park)* **99**, 053838 (2019).
18. Hagemann, J., Töpperwien, M. & Salditt, T. Phase retrieval for near-field X-ray imaging beyond linearisation or compact support. *Appl Phys Lett* **113**, 041109 (2018).

19. Fannjiang, A. & Strohmer, T. The numerics of phase retrieval. *Acta Numerica* **29**, 125–228 (2020).
20. Lecun, Y., Bengio, Y. & Hinton, G. Deep learning. *Nature* vol. 521 436–444 Preprint at <https://doi.org/10.1038/nature14539> (2015).
21. Chen, X., Wei, Z., Li, M. & Rocca, P. A review of deep learning approaches for inverse scattering problems. *Progress in Electromagnetics Research* vol. 167 67–81 Preprint at <https://doi.org/10.2528/PIER20030705> (2020).
22. Midtvedt, B. *et al.* Quantitative digital microscopy with deep learning. *Applied Physics Reviews* vol. 8 011310 Preprint at <https://doi.org/10.1063/5.0034891> (2021).
23. Field, K. G. *et al.* Development and Deployment of Automated Machine Learning Detection in Electron Microscopy Experiments. *Microscopy and Microanalysis* **27**, 2136–2137 (2021).
24. Field, K. G., Shen, M., Massey, C. P., Littrell, K. C. & Morgan, D. D. Rapid Characterization Methods for Accelerated Innovation for Nuclear Fuel Cladding. *Microscopy and Microanalysis* **26**, 868–869 (2020).
25. Jha, D. *et al.* ElemNet: Deep Learning the Chemistry of Materials From Only Elemental Composition. *Sci Rep* **8**, 1–13 (2018).
26. Shen, M. *et al.* A deep learning based automatic defect analysis framework for In-situ TEM ion irradiations. *Comput Mater Sci* **197**, 110560 (2021).
27. Shen, M. *et al.* Multi defect detection and analysis of electron microscopy images with deep learning. *Comput Mater Sci* **199**, 110576 (2021).
28. Sun, X. *et al.* Assessing Graph-based Deep Learning Models for Predicting Flash Point. *Mol Inform* **39**, 1900101 (2020).
29. Jacobs, R. *et al.* Performance and limitations of deep learning semantic segmentation of multiple defects in transmission electron micrographs. *Cell Rep Phys Sci* **3**, (2022).
30. Awe, A. M. *et al.* Machine learning principles applied to CT radiomics to predict mucinous pancreatic cysts. *Abdominal Radiology* **1**, 1–11 (2021).
31. Liu, Y. *et al.* *Harmonization and targeted feature dropout for generalized segmentation: Application to multi-site traumatic brain injury images. Lecture Notes in Computer Science (including subseries Lecture Notes in Artificial Intelligence and Lecture Notes in Bioinformatics)* vol. 11795 LNCS (2019).
32. Gurbani, S. *et al.* Evaluation of radiomics and machine learning in identification of aggressive tumor features in renal cell carcinoma (RCC). *Abdominal Radiology* **46**, 4278–4288 (2021).
33. Konstantinova, T., Wiegart, L., Rakitin, M., DeGennaro, A. M. & Barbour, A. M. Noise reduction in X-ray photon correlation spectroscopy with convolutional neural networks encoder–decoder models. *Sci Rep* **11**, 1–12 (2021).
34. Cherukara, M. J. *et al.* AI-enabled high-resolution scanning coherent diffraction imaging. *Appl Phys Lett* **117**, 044103 (2020).
35. Schloz, M., Müller, J., Pekin, T., Van den Broek, W. & Koch, C. Adaptive Scanning in Ptychography through Deep Reinforcement Learning. *Microscopy and Microanalysis* **27**, 818–821 (2021).

36. Schloz, M., Müller, J., Pekin, T. C., Broek, W. Van den & Koch, C. T. Deep Reinforcement Learning for Data-Driven Adaptive Scanning in Ptychography. (2022) doi:10.48550/arxiv.2203.15413.

37. Oviedo, F. *et al.* Fast and interpretable classification of small X-ray diffraction datasets using data augmentation and deep neural networks. *NPJ Comput Mater* **5**, 1–9 (2019).

38. Ding, J., Li, X., Kang, X. & Gudivada, V. N. A case study of the augmentation and evaluation of training data for deep learning. *Journal of Data and Information Quality* **11**, (2019).

39. Guo, Z. Physics-assisted machine learning for X-ray imaging. (2022).

40. Scheinker, A. & Pokharel, R. Adaptive 3D convolutional neural network-based reconstruction method for 3D coherent diffraction imaging. *J Appl Phys* **128**, 184901 (2020).

41. Guan, Z., Qin, H., Yager, K., Choo, Y. & Yu, D. Automatic X-ray scattering image annotation via double-view Fourier-Bessel convolutional networks. in *British Machine Vision Conference 2018, BMVC 2018* (eds. G. Balint *et al.*) 343–354 (Uniwersytet Śląski. Wydział Matematyki, Fizyki i Chemii, 2019). doi:10.2/JQUERY.MIN.JS.

42. Wu, L. *et al.* Three-dimensional coherent X-ray diffraction imaging via deep convolutional neural networks. *NPJ Comput Mater* **7**, 1–8 (2021).

43. Wu, L., Juhas, P., Yoo, S. & Robinson, I. Complex imaging of phase domains by deep neural networks. *IUCrJ* **8**, 12–21 (2021).

44. Meister, N. *et al.* Robust and scalable deep learning for X-ray synchrotron image analysis. in *2017 New York Scientific Data Summit, NYSDS 2017 - Proceedings* (Institute of Electrical and Electronics Engineers Inc., 2017). doi:10.1109/NYSDS.2017.8085045.

45. Zimmermann, J. *et al.* Deep neural networks for classifying complex features in diffraction images. *Phys Rev E* **99**, 063309 (2019).

46. Liu, J., van der Schot, G. & Engblom, S. Supervised classification methods for flash X-ray single particle diffraction imaging. *Opt Express* **27**, 3884 (2019).

47. Guan, Z. Analysis and Reconstruction of Coherent Diffractive Imaging Using Physics Aware Deep Learning. (2019).

48. Rapaport, D. C. *The Art of Molecular Dynamics Simulation. The Art of Molecular Dynamics Simulation* (Cambridge University Press, 2004). doi:10.1017/CBO9780511816581.

49. Frenkel, D. & Smit, B. *Understanding molecular simulation: From algorithms to applications. Understanding molecular simulation: From algorithms to applications* (2001). doi:10.1063/1.881812.

50. Chan, H. *et al.* BLAST: bridging length/timescales via atomistic simulation toolkit. *MRS Adv* **6**, 21–31 (2021).

51. He, K., Zhang, X., Ren, S. & Sun, J. Identity mappings in deep residual networks. in *Lecture Notes in Computer Science (including subseries Lecture Notes in Artificial Intelligence and Lecture Notes in Bioinformatics)* vol. 9908 LNCS 630–645 (Springer Verlag, 2016).

52. He, K., Zhang, X., Ren, S. & Sun, J. Deep residual learning for image recognition. in *Proceedings of the IEEE Computer Society Conference on Computer Vision and Pattern Recognition* vols 2016-Decem 770–778 (IEEE Computer Society, 2016).

53. Shrestha, A. & Mahmood, A. Review of Deep Learning Algorithms and Architectures. *IEEE Access* **7**, 53040–53065 (2019).
54. Russakovsky, O. *et al.* Imagenet large scale visual recognition challenge. *Int J Comput Vis* **115**, 211–252 (2015).
55. Chollet, F. *Deep Learning with Python*. *Shelter Island, NY: Manning Publications Co.*, [2018] ©2018 (Manning Publications Co, 2018).
56. Abadi, M. *et al.* TensorFlow: A System for Large-Scale Machine Learning. in *12th USENIX Symposium on Operating Systems Design and Implementation (OSDI '16)* 265–284 (2016). doi:10.1038/nn.3331.
57. Simonyan, K., Vedaldi, A. & Zisserman, A. Deep inside convolutional networks: Visualising image classification models and saliency maps. in *2nd International Conference on Learning Representations, ICLR 2014 - Workshop Track Proceedings* (International Conference on Learning Representations, ICLR, 2014). doi:10.48550/arxiv.1312.6034.
58. Selvaraju, R. R. *et al.* Grad-CAM: Visual Explanations from Deep Networks via Gradient-Based Localization. *Proceedings of the IEEE International Conference on Computer Vision 2017-October*, 618–626 (2017).
59. Zhang, Y. *et al.* Grad-CAM helps interpret the deep learning models trained to classify multiple sclerosis types using clinical brain magnetic resonance imaging. *J Neurosci Methods* **353**, 109098 (2021).
60. Yosinski, J., Clune, J., Nguyen, A., Fuchs, T. & Lipson, H. Understanding Neural Networks Through Deep Visualization. (2015) doi:10.48550/arxiv.1506.06579.
61. Pokuri, B. S. S., Ghosal, S., Kokate, A., Sarkar, S. & Ganapathysubramanian, B. Interpretable deep learning for guided microstructure-property explorations in photovoltaics. *NPJ Comput Mater* **5**, 1–11 (2019).
62. Koppula, S. *et al.* A Deep Learning Approach for Characterizing Major Galaxy Mergers. (2021) doi:10.48550/arxiv.2102.05182.
63. Crocker, J. C. & Grier, D. G. Methods of Digital Video Microscopy for Colloidal Studies. *J Colloid Interface Sci* **179**, 298–310 (1996).

Supplemental Information

This supplemental information describes the Saliency Maps and Gradient-weighted Class Activation Mapping (Grad-CAM) for the test images categorized in this work (see main text for more information). The data is available in digital form on FigShare at the DOI provided in the “Data and Code Availability” section of the main text. Each numbered item below describes one set of data and then the folder where it can be found. Each folder has Saliency Maps or Grad-CAM for 1900 images. These folders are in the file “Paper_SI.zip”.

- 1) Grad-CAM of non-Polydispersity System for speckle pattern image size 513 x 513: CAM/Non-Poly/size513.
- 2) Grad-CAM of non-Polydispersity System for speckle pattern image size 257 x 257: CAM/Non-Poly/size257
- 3) Grad-CAM of Polydispersity System: CAM/Poly/CAM
- 4) Saliency Map of non-Polydispersity System for speckle pattern image size 513 x 513: Saliency/Non-Poly/size513
- 5) Saliency Map of non-Polydispersity System for speckle pattern image size 257 x 257: Saliency/Non-Poly/size257
- 6) Saliency Map of Polydispersity System: Saliency/Poly/Saliency